Mon. Not. R. Astron. Soc. **386,** 2311–2322 (2008) doi:10.1111/j.1365-2966.2008.13211.x

# Galaxy populations in the Antlia cluster – I. Photometric properties of early-type galaxies*

Analía V. Smith Castelli,[1,2]† Lilia P. Bassino,[1,2]† Tom Richtler,[3]† Sergio A. Cellone,[1,2]† Cristian Aruta‡ and Leopoldo Infante[4]†

[1]*Facultad de Ciencias Astronómicas y Geofísicas, Universidad Nacional de La Plata, Paseo del Bosque, B1900FWA La Plata, Argentina*
[2]*Instituto de Astrofísica de la Plata (CONICET-UNLP)*
[3]*Departamento de Física, Universidad de Concepción, Casilla 160-C, Concepción, Chile*
[4]*Departamento de Astronomía y Astrofísica, Pontificia Universidad Católica de Chile, Casilla 306, Santiago 22, Chile*

Accepted 2008 March 7. Received 2008 March 6; in original form 2007 November 16

**ABSTRACT**

We present the first colour–magnitude relation (CMR) of early-type galaxies in the central region of the Antlia cluster, obtained from CCD wide-field photometry in the Washington photometric system. Integrated $(C - T_1)$ colours, $T_1$ magnitudes, and effective radii have been measured for 93 galaxies (i.e. the largest galaxies sample in the Washington system till now) from the FS90 Antlia Group catalogue. Membership of 37 objects can be confirmed through new radial velocities and data collected from the literature. The resulting colour–magnitude diagram shows that early-type FS90 galaxies that are spectroscopically confirmed Antlia members or that were considered as definite members by FS90, follow a well-defined CMR [$\sigma_{(C-T_1)} \sim 0.07$ mag] that spans 9 mag in brightness with no apparent change of slope. This relation is very tight for the whole magnitude range but S0 galaxies show a larger dispersion, apparently due to a separation of ellipticals and S0s. Antlia displays a slope of $-13.6$ in a $T_1$ versus $(C - T_1)$ diagram, in agreement with results for clusters like Fornax, Virgo, Coma and Perseus, which are dynamically different to Antlia. This fact might indicate that the build-up of the CMR in cluster of galaxies is more related to galaxies internal processes than to the influence of the environment. Interpreting the CMR as a luminosity–metallicity relation of old stellar systems, the metallicities of the Antlia galaxies define a global relation down to $M_V \approx -13$. We also find, for early-type dwarfs, no clear relation between luminosity and effective radius, indicating a nearly constant mean effective radius of $\sim$1 kpc. This value is also found in several samples of dwarf galaxies in Virgo and Coma.

**Key words:** galaxies: clusters: general – galaxies: clusters: individual: Antlia – galaxies: dwarf – galaxies: elliptical and lenticular, CD – galaxies: photometry.

## 1 INTRODUCTION

It is well known that early-type galaxies in clusters and groups define a tight sequence in the colour–magnitude diagram (CMD), in the sense that more luminous ellipticals (Es) are redder than fainter ones (e.g. Baum 1959; De Vaucouleurs 1961; Visvanathan & Sandage 1977; Bower, Lucey & Ellis 1992; Carrasco, Mendes de Oliveira & Infante 2006). Many spectroscopic studies of giant Es (e.g. Kuntschner 2000, for the Fornax cluster; Vazdekis et al. 2001, for the Virgo cluster; see also Terlevich & Forbes 2002; Chang et al. 2006) and dwarf galaxies (e.g. Carter et al. 2002; Thomas et al. 2003a; Thomas, Maraston & Bender 2003b; van Zee, Barton & Skillman 2004; Mieske et al. 2007) have shown that the colour–magnitude relation (CMR) mainly reflects metallicity effects. A reasonable explanation, which comes from an analysis of the CMR, is based on the assumption that the more luminous (massive) galaxies, capable of retaining their metal content due to their deep potential wells, can be enriched to higher levels than low-mass Es which are more sensitive to the effect of mass-loss by galactic winds and supernovae (Dressler 1984; Kodama & Arimoto 1997; Rakos et al. 2001, and references therein). In a cluster environment, tidal stripping of

*This paper is based on data obtained with the 4-m telescope at CTIO, Chile, with the 6.5-m Magellan telescopes at Las Campanas Observatory, Chile, and at CASLEO, operated under agreement between CONICET and the Universities of La Plata, Córdoba and San Juan, Argentina.

†E-mail: asmith@fcaglp.unlp.edu.ar (AVSC); lbassino@fcaglp.unlp.edu.ar (LPB); tom@mobydick.cfm.udec.cl (TR); scellone@fcaglp.unlp.edu.ar (SAC); linfante@astro.puc.cl (LI)
‡In memoriam.

© 2008 The Authors. Journal compilation © 2008 RAS

gas and/or interaction with the intracluster medium might also play a role. See De Rijcke et al. (2005) for an account of theoretical models.

Although also early-type dwarf galaxies in clusters and groups seem to follow a well-defined CMR (Caldwell 1983; Secker, Harris & Plummer 1997; Hilker, Mieske & Infante 2003; López-Cruz, Barkhouse & Yee 2004; Carrasco et al. 2006; Mieske et al. 2007; Lisker, Grebel & Binggeli 2008), it is not yet clear whether this relation broadens towards fainter magnitudes (Conselice, Gallagher & Wyse 2002, 2003) or just extends the one followed by the Es (Adami et al. 2006; Andreon et al. 2006) with a similar slope and level of scatter. Bower et al. (1992) report that the CMR defined by the luminous early-type galaxies has the same form in the Virgo and Coma clusters, even using different colours ($U-V, V-K$ or $J-K$) versus the total $V$ magnitude. Lisker, Grebel & Binggeli (2005) (see also Lisker et al. 2008) have shown that nucleated dEs in Virgo follow a tight CMR with no broadening towards fainter magnitudes, which extends to brighter Es but with a change in slope. Furthermore, these authors point out that dS0 should be considered as a separate class of dwarf galaxies in order to properly analyse CMDs.

Terlevich, Caldwell & Bower (2001) perform an ($U$, $V$) photometric study of galaxies in the Coma cluster to investigate the dependence of the slope and dispersion of the CMR on the morphology and luminosity of the galaxies, and on their environmental properties within the cluster. They find the CMR to be consistent when compared between samples of early-type galaxies with different characteristics. In particular, no variation in the CMR slope between E and S0 galaxies is detected.

However, a common and well-defined CMR of early-type galaxies over a broad magnitude range seems to be surprising, given that the chemical histories of giant Es and dwarf galaxies have supposedly been quite different. The $\alpha$-element overabundance of giant Es points to post-starburst populations, rapidly enriched by type II supernovae, while the subsolar $\alpha$ abundances of dwarf galaxies rather speak for a continuous enrichment, which has ceased because of gas removal by galactic outflows or stripping (Thomas et al. 2003b; van Zee et al. 2004; for an alternative view, see also Köppen, Weidner & Kroupa 2007).

In this context, nearby galaxy clusters are obviously of particular interest. We have started the Antlia Cluster Project whose goal is to study the galaxy population of the Antlia cluster, which is the third nearest well-populated galaxy cluster after those of Virgo and Fornax. Despite its proximity, richness and concentration, Antlia is until now practically unexplored. It is located between the third and fourth Galactic quadrants, not too far from the Galactic plane ($l \approx 270^\circ, b \approx 20^\circ$).

Antlia exhibits a complex structure consisting of several subgroups, the most conspicuous ones being dominated by the giant elliptical galaxies NGC 3258 and 3268. X-ray observations showed extended emission around both subgroups (Pedersen, Yoshii & Sommer-Larsen 1997; Nakazawa et al. 2000). The gravitating masses estimated in these studies for each group are of the order of $1.9 \times 10^{13}$ $M_\odot$ within a radius of $\sim$250 kpc, i.e. similar to what is found in Fornax within the same radius. In both subgroups, the emission is concentrated towards the dominant galaxy, but extensions elongated in the direction to the other subgroup are also present. This kind of substructure depicted in X-rays suggests an ongoing merger.

Here, we shall adopt the distance modulus $(m-M) = 32.73$ given by Dirsch, Richtler & Bassino (2003), which was calculated as the mean of the distances towards the two giant Es obtained by Prugniel & Simien (1996) and Tonry et al. (2001). According to the distance moduli estimated for both giants with the surface brightness fluctuation (SBF) method by Tonry et al., they are separated by about 3 Mpc, but this difference is not conclusive because their distance moduli as well as their radial velocities agree within the errors.

Dirsch et al. (2003) performed the first investigation of the globular cluster (GC) systems around NGC 3258 and 3268. They showed that both cluster systems are elongated in the same direction as a connecting line between the two galaxies, resembling the X-ray results. More recent results on these GC systems can be found in Harris et al. (2006) and Bassino, Richtler & Dirsch (2008), who show that the GC systems colour distributions are bimodal but the brightest GCs present a unimodal distribution. Furthermore, the red (metal-rich) GCs follow closely the galaxies' surface brightness profiles, and the estimated total GC populations are $6000 \pm 150$ GCs for NGC 3258 and $4750 \pm 150$ GCs for NGC 3268.

The photographic work of Ferguson & Sandage (1990) was the first and last major effort devoted to study the galaxy population of the Antlia cluster. They identified, by visual inspection of photographic plates, 375 galaxies that are listed in their Antlia Group Catalogue (named hereafter with the acronym FS90 plus the catalogue number). It gives, among other data, a membership status (1. definite member, 2. likely member, 3. possible member) and a morphological type for each galaxy. The membership status was mainly based on morphological criteria, i.e. surface brightness, resolution into knots and late-type galaxies' luminosity class (see Binggeli, Sandage & Tammann 1985, for more details), as only about 6 per cent of the galaxies in this catalogue had available radial velocities. They showed that the central galaxy density in Antlia is a factor of 1.4 higher than in Fornax, and 1.7 higher than in Virgo.

In this first paper of the Antlia Cluster Project, we present initial results from a photometric study, using the Washington photometric system (Canterna 1976), of 100 FS90 galaxies in the central region of the cluster. To our knowledge, this galaxy sample is the largest one studied with the Washington system till now. We also add some new radial velocities for several galaxies. In Section 2, we give information about the photometric and spectroscopic observations, as well as the data. In Section 3, we show the CMD and the surface brightness–luminosity diagram for 93 FS90 galaxies placed in the central region of Antlia. We present a discussion of our work in Section 4 and, in Section 5, our conclusions.

## 2 DATA AND REDUCTION

The photometric observations were performed with the MOSAIC camera (eight CCDs mosaic imager) mounted at the prime focus of the 4-m Blanco telescope at the Cerro Tololo Inter-American Observatory (CTIO), during 2002 April 4–5. One pixel of the MOSAIC wide-field camera subtends 0.27 arcsec on the sky, which results in a field of $36 \times 36$ arcmin$^2$, about $370 \times 370$ kpc$^2$ at the Antlia distance (35.2 Mpc). The central part of the cluster has been covered by one MOSAIC field (Fig. 1), with both short and long exposures. The same material has already been used to investigate the GC systems of the dominant elliptical galaxies. Details are given in Dirsch et al. (2003).

Kron–Cousins $R$ and Washington $C$ filters were used. We selected the $R$ filter instead of the original Washington $T_1$ as Geisler (1996) has shown that the Kron–Cousins $R$ filter is more efficient than $T_1$, as it has a better transmission at all wavelengths, and that $R$ and $T_1$ magnitudes are very similar, with just a very small colour term and

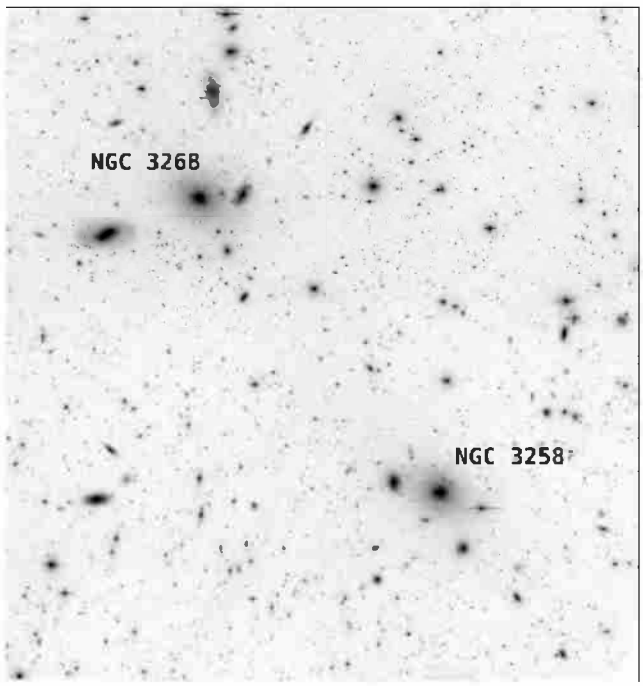


**Figure 1.** $C + R$ combined image of the MOSAIC field. Labels indicate the two dominant galaxies of the Antlia cluster. North is up and east is towards the left-hand side.

zero-point difference ($R - T_1 \approx -0.02$). The seeing on the $R$ image is 1 arcsec and on the $C$ image is 1.1 arcsec.

Medium-resolution spectroscopic observations were performed during two nights (2004 January 19–20) with the IMACS areal camera and spectrograph mounted on the Magellan I Baade 6.5-m Telescope (Las Campanas Observatory, Chile). Additional low-resolution spectra for three FS90 blue compact dwarf (BCD) candidates were obtained during the nights of 2007 March 12–13, with the REOSC spectrograph at the 'Jorge Sahade' 2.15-m telescope of La Plata University, Argentina. Radial velocities were measured by cross-correlation and, in the case of BCDs, by fitting bright emission lines. Details will be given in Smith Castelli et al. (in preparation).

A total of 100 galaxies from the FS90 Antlia Group Catalogue are located in our field. The brightest ones are overexposed in our long-exposure frames. To obtain colours and magnitudes for the non-overexposed FS90 galaxies, we ran SEXTRACTOR (Bertin & Arnouts 1996) on our long-exposure $R$ frame. We considered as detection criteria 10 connected pixels above $1.5\sigma$ of the background level. A pyramidal filter was applied and the global background map used for detection was constructed by setting a mesh size of $64 \times 64$ pixel$^2$ ($\sim 17 \times 17$ arcsec$^2$). To obtain accurate photometry, we used the local background option of SEXTRACTOR by setting rectangular annuli with widths of 24 pixels around the objects (Bertin & Arnouts 1996). We adopted MAG_AUTO, i.e. a Kron-like elliptical aperture magnitude, as a representative total magnitude of the detected objects in both filters (Nonino et al. 1999). To get $(C - T_1)$ colours in a consistent manner, the corresponding $C$ magnitudes were measured using the same coordinates and Kron-like elliptical apertures obtained from the $R$ image.

In order to obtain integrated magnitudes and colours for faint objects that were not properly detected by SEXTRACTOR, as well as for the brightest galaxies whose centres are overexposed on the long-exposure frames, we worked with the task ELLIPSE within IRAF (more details will be given in Smith Castelli et al., in preparation). In all these cases, we used smaller trimmed images in both filters, containing the target galaxies, and measured the background locally. Note that in the case of the brightest galaxies, the use of MAG_AUTO would have lead to a severe underestimation of the light of the galaxy (Graham & Driver 2005). For fainter objects (i.e. those displaying rather exponential profiles), however, total magnitudes obtained from Kron-like elliptical apertures can be considered as representative of the total luminosity of the galaxy, as stated by Graham & Driver.

As said above, for each faint object not detected by SEXTRACTOR we have used trimmed and registered images of the same sizes in $R$ and $C$ filters. We estimated the sky level from the statistic provided by IMEXA. After subtracting the sky level and masking foreground stars, we run ELLIPSE on the $R$ image. The photometry of the sky subtracted $C$ image was obtained considering the same elliptical apertures of the $R$ image with the aim at estimating consistent colours. Once we obtained the photometry in both filters, we corrected the sky level by constructing growth curves, i.e. we plotted the integrated flux within the elliptical apertures versus the semimajor axis of the apertures. The correction to the sky level of an image is the value for which these curves display an asymptotic flat behaviour to infinity. Therefore, we added or subtracted different constant values (smaller than 2 per cent of the original estimated level) to the integrated fluxes until we got asymptotically flat curves. These corrected fluxes provided the brightness profiles that were numerically integrated to obtain the integrated magnitudes in each filter. From these magnitudes we calculated the integrated colours.

For the galaxies with overexposed centres, we considered long and short-exposure images in both filters. We rescaled the intensities of the short-exposure images to the long-exposure ones, performed internal fits on the sky subtracted short-exposure $R$ images and external fits on the sky subtracted long-exposure ones. We then used the corresponding elliptical apertures to perform the photometry on the sky subtracted short and long-exposure $C$ images. To obtain the whole brightness profile in each filter, we merged the internal and external fits, and we corrected the external sky level as it had been calculated for faint objects. Again, the corrected fluxes provided the brightness profiles that were numerically integrated to obtain total magnitudes and colours.

Magnitude and colour errors were estimated using the equations given by Lisker et al. (2008) in their section 4, but omitting the last term in equation (3) (we note that this equation refers to a relative flux error). In our case, the uncertainty in the sky level determination per pixel is taken to be 8 per cent, as it is obtained from our images. Following Lisker et al., we also consider the flux uncertainty caused by the uncertainty in the semimajor axis of our elliptical apertures to be similar to that of the sky level.

The FS90 number, NGC number, J2000 coordinates, FS90 morphology and membership status, and $E(B - V)$ values for 100 FS90 galaxies are listed in Table 1 in the first seven columns. The eighth and ninth columns give the total magnitude and colour (not corrected by absorption or reddening), respectively, with errors in parenthesis. The tenth column gives the surface brightness of the limiting isophote, within which the total magnitude has been calculated. The 11th column lists the corresponding limiting radius. The 12th column gives the mean surface brightness within the effective radius (i.e. the radius containing half of the light), and the 13th column the effective radius measured in the $R$ band. The 14th column gives the heliocentric radial velocities derived from our spectra, as well as

**Table 1.** FS90 galaxies in our MOSAIC field of the central Antlia region.

| FS90 ID | NGC | FS90 $\alpha$ (2000) | FS90 $\delta$ (2000) | FS90 mor. | FS90 status | $E(B-V)$ | $T_1$ (mag) | $(C-T_1)$ (mag) | $\mu_{T_1}$ (mag arcsec$^{-2}$) | $r_{T_1}$ (arcsec) | $\langle\mu_{\rm eff}\rangle$ (mag arcsec$^{-2}$) | $r_{\rm eff}$ (arcsec) | $v_r$ (km s$^{-1}$) | Remarks |
|---|---|---|---|---|---|---|---|---|---|---|---|---|---|---|
| 68 | | 10:28:03.1 | −35:26:31 | SBab | 2 | 0.080 | 14.38 (0.01) | 1.60 (0.02) | 25.8 | 18.8 | 21.4 | 10.3 | $3189 \pm 80$[1] | SE |
| 69 | | 10:28:05.0 | −35:28:55 | dE | 2 | 0.081 | 18.88 (0.02) | 1.60 (0.04) | 25.7 | 7.5 | 23.3 | 3.1 | | SE, DM |
| 70 | | 10:28:06.9 | −35:35:20 | dE | 1 | 0.078 | 17.76 (0.02) | 1.64 (0.04) | 25.7 | 12.3 | 23.4 | 5.4 | | SE |
| 71 | | 10:28:07.9 | −35:37:26 | Sd | 1 | 0.076 | 16.31 (0.01) | 0.88 (0.02) | 25.8 | 13.6 | 22.3 | 6.2 | | SE |
| 72 | | 10:28:07.9 | −35:38:20 | S0 | 1 | 0.075 | 14.39 (0.01) | 1.95 (0.02) | 25.7 | 16.9 | 20.4 | 6.4 | $3114 \pm 80$[1] | SE |
| | | | | | | | | | | | | | $2986 \pm 38$[3] | |
| 73 | | 10:28:09.8 | −35:43:04 | dE | 1 | 0.073 | 16.97 (0.01) | 1.70 (0.02) | 25.7 | 10.5 | 22.2 | 4.4 | | SE |
| 75 | | 10:28:12.0 | −35:32:20 | BCD? | 3 | 0.081 | 17.65 (0.01) | 1.01 (0.02) | 25.7 | 4.0 | 20.7 | 1.6 | $12\,450 \pm 95$[3] | SE |
| 76 | | 10:28:12.9 | −35:35:38 | dE | 2 | 0.079 | 18.04 (0.01) | 1.44 (0.02) | 25.8 | 5.4 | 22.2 | 2.7 | $25\,298 \pm 45$[3] | SE |
| 77 | | 10:28:15.1 | −35:32:02 | dE, N pec or Amorphous? | 2 | 0.081 | 14.78 (0.01) | 1.80 (0.02) | 28.9 | 33.4 | 21.2 | 7.8 | $2382 \pm 49$[3] | ELL, NS |
| 78 | | 10:28:15.8 | −35:46:26 | dE | 1 | 0.076 | 19.36 (0.06) | 2.01 (0.06) | 27.4 | 10.8 | 24.5 | 4.3 | | ELL |
| 79 | 3258A | 10:28:19.2 | −35:27:21 | S0 | 1 | 0.082 | 13.20 (0.01) | 2.09 (0.02) | 27.9 | 50.7 | 19.6 | 7.5 | $2930 \pm 60$[1] | ELL, NS |
| | | | | | | | | | | | | | $2734 \pm 36$[3] | |
| 80 | | 10:28:18.9 | −35:45:28 | dS0 | 1 | 0.075 | 13.80 (0.01) | 2.08 (0.02) | 28.3 | 46.5 | 19.4 | 5.2 | $2544 \pm 80$[2] | ELL, NS |
| 82 | | 10:28:23.0 | −35:29:56 | S? or dS0? | 3 | 0.082 | 16.22 (0.02) | 2.34 (0.03) | 28.7 | 19.8 | 20.8 | 3.3 | $19\,577 \pm 41$[1] | ELL, DM |
| | | | | | | | | | | | | | $19\,512 \pm 52$[3] | |
| 83 | | 10:28:23.0 | −35:30:57 | S or Sm | 3 | 0.082 | 16.31 (0.01) | 1.45 (0.02) | 25.7 | 11.9 | 21.8 | 5.0 | | SE |
| 84 | | 10:28:24.0 | −35:31:40 | E | 2 | 0.082 | 13.70 (0.01) | 2.04 (0.02) | 28.3 | 42.3 | 19.4 | 5.4 | $2457 \pm 80$[2] | ELL, NS |
| 85 | | 10:28:24.0 | −35:34:22 | dE | 1 | 0.081 | 18.12 (0.04) | 1.60 (0.07) | 25.6 | 14.6 | 23.9 | 5.6 | | SE |
| 87 | | 10:28:25.2 | −35:14:34 | dE, N | 1 | 0.091 | 15.75 (0.01) | 1.87 (0.02) | 25.7 | 16.4 | 22.2 | 7.9 | | SE, DM |
| 88 | | 10:28:28.0 | −35:31:04 | S or Sm | 3 | 0.083 | 15.05 (0.01) | 1.79 (0.02) | 28.5 | 21.9 | 19.7 | 3.5 | $19\,659 \pm 80$[2] | ELL |
| 93 | | 10:28:31.9 | −35:40:40 | SmV | 1 | 0.075 | 15.96 (0.01) | 0.91 (0.02) | 25.8 | 18.7 | 22.7 | 9.0 | | SE |
| 94 | | 10:28:31.9 | −35:42:21 | S0 | 1 | 0.074 | 13.22 (0.01) | 1.99 (0.02) | 28.6 | 44.0 | 17.9 | 3.5 | $2826 \pm 80$[2] | ELL |
| 95 | | 10:28:34.0 | −35:31:22 | dE | 2 | 0.084 | 19.95 (0.04) | 1.57 (0.06) | 25.8 | 5.9 | 24.3 | 2.9 | | SE |
| 98 | | 10:28:35.0 | −35:27:39 | BCD | 3 | 0.085 | 15.94 (0.01) | 1.25 (0.02) | 25.8 | 8.2 | 20.1 | 2.7 | $2890 \pm 94$[3] | SE |
| 103 | | 10:28:45.1 | −35:34:40 | dE | 3 | 0.084 | 19.95 (0.03) | 1.57 (0.04) | 25.8 | 4.9 | 23.8 | 2.3 | | SE |
| 105 | 3257 | 10:28:48.0 | −35:39:28 | SB01 | 1 | 0.077 | 12.77 (0.01) | 2.04 (0.02) | 28.2 | 69.4 | 18.6 | 5.8 | $3200 \pm 26$[1] | ELL |
| 106 | | 10:28:51.3 | −35:09:39 | BCD? | 3 | 0.098 | 17.10 (0.01) | 0.96 (0.02) | 25.8 | 8.7 | 21.6 | 3.1 | $2409 \pm 115$[3] | SE |
| 108 | | 10:28:53.2 | −35:19:12 | d:E, N | 1 | 0.092 | 14.73 (0.02) | 2.03 (0.03) | 28.3 | 39.6 | 21.2 | 7.8 | $2611 \pm 39$[3] | ELL, NS |
| 109 | | 10:28:53.0 | −35:32:52 | dE | 2 | 0.087 | 18.99 (0.03) | 1.64 (0.05) | 28.0 | 7.6 | 23.1 | 2.6 | | ELL, NS |
| 110 | | 10:28:53.0 | −35:35:34 | E(M32?) | 3 | 0.085 | 15.49 (0.01) | 2.06 (0.02) | 27.5 | 14.0 | 18.4 | 1.5 | | ELL |
| 111 | 3258 | 10:28:54.0 | −35:36:21 | E | 1 | 0.084 | 10.89 (0.01) | 2.18 (0.02) | 28.1 | 188.5 | 20.1 | 28.5 | $2792 \pm 28$[1] | ELL |
| | | | | | | | | | | | | | $2689 \pm 50$[3] | |
| 114 | | 10:28:56.1 | −35:27:39 | dE | 1 | 0.088 | 19.81 (0.06) | 1.45 (0.08) | 25.8 | 7.4 | 24.4 | 3.4 | | SE |
| 115 | | 10:28:57.1 | −35:33:39 | dE | 2 | 0.088 | 19.04 (0.04) | 1.64 (0.06) | 25.8 | 8.8 | 24.1 | 4.1 | | SE |
| 118 | | 10:28:58.3 | −35:09:36 | dE | 1 | 0.097 | 18.67 (0.06) | 1.71 (0.10) | 25.8 | 13.4 | 25.1 | 7.7 | | SE |
| 120 | | 10:29:02.1 | −35:34:04 | ImV | 1 | 0.088 | 16.38 (0.02) | 1.28 (0.02) | 25.8 | 17.4 | 22.8 | 7.6 | | SE |
| 121 | | 10:29:02.1 | −35:35:34 | dE? | 3 | 0.087 | – | – | – | – | – | – | – | DC |
| 123 | | 10:29:03.1 | −35:40:30 | dE, N | 2 | 0.080 | 16.33 (0.01) | 1.71 (0.02) | 25.8 | 12.5 | 21.9 | 5.1 | | SE |
| 125 | 3260 | 10:29:06.2 | −35:35:34 | S02 | 1 | 0.087 | 12.28 (0.01) | 2.12 (0.02) | 27.8 | 66.3 | 19.4 | 10.5 | $2416 \pm 32$[1] | ELL, DM |
| | | | | | | | | | | | | | $2439 \pm 46$[3] | |
| 131 | | 10:29:11.0 | −35:41:24 | Sb(r) | 3 | 0.081 | 14.26 (0.01) | 1.21 (0.02) | 25.8 | 16.4 | 20.5 | 7.1 | $2104 \pm 60$[3] | SE |
| 133 | | 10:29:12.0 | −35:39:28 | d:E, N | 1 | 0.083 | 14.63 (0.01) | 1.87 (0.02) | 25.8 | 16.5 | 20.6 | 6.4 | | SE |
| 134 | | 10:29:13.2 | −35:29:24 | S0 | 2 | 0.089 | 14.23 (0.01) | 1.89 (0.02) | 27.2 | 40.0 | 19.7 | 4.9 | $1355 \pm 60$[3] | ELL |
| 136 | | 10:29:15.3 | −35:25:58 | dE, N | 1 | 0.090 | 16.12 (0.01) | 1.86 (0.02) | 25.8 | 14.5 | 21.9 | 5.9 | | SE |
| 137 | | 10:29:15.1 | −35:41:34 | ImV | 2 | 0.081 | 17.74 (0.02) | 0.81 (0.03) | 25.8 | 11.6 | 23.8 | 6.5 | | SE |
| 140 | | 10:29:18.2 | −35:35:06 | dE, N | 2 | 0.090 | 16.90 (0.02) | 1.88 (0.03) | 25.8 | 14.0 | 23.2 | 7.3 | | SE |
| 142 | | 10:29:20.1 | −35:35:09 | dS0? | 2 | 0.090 | 15.70 (0.01) | 1.85 (0.02) | 25.8 | 14.0 | 21.5 | 5.7 | | SE |
| 144 | | 10:29:22.5 | −35:09:21 | dE | 2 | 0.100 | 19.13 (0.04) | 1.56 (0.05) | 25.8 | 8.2 | 24.1 | 4.0 | | SE |
| 148 | | 10:29:27.3 | −35:24:35 | dE/Im | 3 | 0.093 | – | – | – | – | – | – | – | NS |
| 149 | | 10:29:27.3 | −35:27:10 | S0 or dS0 | 3 | 0.091 | 16.95 (0.01) | 2.54 (0.02) | 25.8 | 5.7 | 20.5 | 2.1 | | SE, DM |
| 153 | | 10:29:31.4 | −35:15:39 | S0 | 1 | 0.101 | 13.24 (0.02) | 1.98 (0.03) | 28.4 | 50.4 | 18.7 | 4.9 | $1852 \pm 37$[1] | ELL |
| | | | | | | | | | | | | | $1733 \pm 39$[3] | |
| 154 | | 10:29:31.4 | −35:10:33 | dE/ImV | 1 | 0.102 | 17.78 (0.10) | 1.92 (0.14) | 28.2 | 25.5 | 24.4 | 9.5 | | ELL, NS |
| 159 | | 10:29:41.5 | −35:17:31 | d:E, N? | 1 | 0.100 | 16.12 (0.01) | 1.80 (0.02) | 25.8 | 10.5 | 21.4 | 4.5 | | SE |
| 160 | | 10:29:41.0 | −35:45:36 | dE | 1 | 0.085 | 18.46 (0.05) | 1.73 (0.09) | 25.8 | 13.7 | 24.8 | 7.3 | | SE |
| 162 | | 10:29:43.4 | −35:29:49 | dE, N | 1 | 0.091 | 17.06 (0.02) | 1.75 (0.03) | 25.8 | 13.8 | 22.9 | 5.9 | | SE |
| 164 | | 10:29:46.5 | −35:13:22 | ? or dE | 3 | 0.104 | 18.37 (0.04) | 1.59 (0.06) | 25.8 | 12.3 | 24.2 | 5.8 | | SE |
| 165 | | 10:29:46.0 | −35:42:25 | S0(M32?) | 3 | 0.086 | 15.50 (0.01) | 2.01 (0.02) | 28.7 | 20.9 | 20.3 | 3.6 | $2605 \pm 80$[2] | ELL |

**Table 1** – *continued*

| FS90 ID | NGC | FS90 $\alpha$ (2000) | FS90 $\delta$ (2000) | FS90 mor. | FS90 status | $E(B-V)$ | $T_1$ (mag) | $(C-T_1)$ (mag) | $\mu_{T_1}$ (mag arcsec$^{-2}$) | $r_{T_1}$ (arcsec) | $\langle\mu_{\rm eff}\rangle$ (mag arcsec$^{-2}$) | $r_{\rm eff}$ (arcsec) | $v_r$ (km s$^{-1}$) | Remarks |
|---|---|---|---|---|---|---|---|---|---|---|---|---|---|---|
| 166 | | 10:29:47.5 | −35:24:10 | E | 2 | 0.097 | 15.28 (0.02) | 2.35 (0.04) | 28.9 | 30.8 | 20.4 | 4.3 | 18 658 ± 99[3] | ELL |
| 168 | 3267 | 10:29:48.4 | −35:19:22 | SB01/2 | 1 | 0.100 | 12.37 (0.01) | 2.16 (0.02) | 28.6 | 53.4 | 19.7 | 11.5 | 3709 ± 33[1] | ELL, DM |
| | | | | | | | | | | | | | 3773 ± 65[3] | |
| 169 | | 10:29:48.4 | −35:25:12 | E | 1 | 0.096 | – | – | – | – | – | – | 3027 ± 80[2] | GAP |
| | | | | | | | | | | | | | 2999 ± 37[3] | |
| 173 | | 10:29:51.6 | −35:10:04 | d:E | 1 | 0.105 | 13.93 (0.01) | 2.04 (0.02) | 27.6 | 33.1 | 19.7 | 5.8 | 2650 ± 80[2] | ELL, NS |
| 174 | | 10:29:52.0 | −35:46:22 | ? or dE, N | 3 | 0.087 | 18.77 (0.02) | 1.75 (0.03) | 25.8 | 6.2 | 23.1 | 2.9 | | SE |
| 175 | | 10:29:53.5 | −35:22:37 | d:SB01 | 1 | 0.100 | 14.00 (0.01) | 2.00 (0.02) | 28.5 | 45.0 | 20.5 | 8.1 | 1781 ± 66[1] | ELL |
| | | | | | | | | | | | | | 1766 ± 98[3] | |
| 176 | | 10:29:54.4 | −35:17:16 | dE, N | 1 | 0.102 | 17.24 (0.01) | 1.71 (0.02) | 25.8 | 10.6 | 22.4 | 4.3 | | SE |
| 177 | | 10:29:54.4 | −35:19:19 | d:E, N | 1 | 0.101 | 15.52 (0.01) | 1.83 (0.02) | 25.8 | 12.1 | 21.1 | 5.2 | 3559 ± 80[2] | SE |
| | | | | | | | | | | | | | 3505 ± 45[3] | |
| 178 | | 10:29:56.4 | −35:26:13 | dE | 3 | 0.096 | – | – | – | – | – | – | – | DC |
| 179 | | 10:29:56.4 | −35:31:40 | dE? | 3 | 0.092 | 18.76 (0.01) | 1.84 (0.02) | 25.8 | 4.4 | 22.6 | 2.4 | 56 125 ± 55[3] | SE |
| 182 | | 10:29:57.1 | −35:42:46 | dE | 3 | 0.088 | 18.77 (0.03) | 1.65 (0.04) | 25.8 | 8.6 | 23.8 | 4.0 | | SE |
| 184 | 3269 | 10:29:57.6 | −35:13:30 | S0/a | 1 | 0.104 | 11.84 (0.01) | 2.01 (0.02) | 28.8 | 84.5 | 19.4 | 13.0 | 3754 ± 33[1] | ELL, DM, NS |
| | | | | | | | | | | | | | 3753 ± 99[3] | |
| 185 | 3268 | 10:29:58.5 | −35:19:30 | E | 1 | 0.103 | 10.76 (0.01) | 2.23 (0.02) | 27.1 | 192.3 | 20.7 | 39.5 | 2800 ± 21[1] | ELL |
| 186 | | 10:29:59.5 | −35:18:10 | dE | 1 | 0.102 | 18.67 (0.02) | 1.66 (0.03) | 25.8 | 7.4 | 23.6 | 3.9 | | SE |
| 188 | | 10:30:02.4 | −35:24:28 | dE | 1 | 0.101 | 18.03 (0.02) | 1.78 (0.03) | 25.8 | 8.4 | 23.2 | 4.4 | | SE, DM |
| 189 | | 10:30:02.4 | −35:36:36 | dE/Im | 2 | 0.094 | 18.31 (0.03) | 1.86 (0.04) | 25.8 | 9.9 | 23.6 | 4.7 | | SE, DM |
| 192 | | 10:30:04.5 | −35:20:31 | E(M32?) | 3 | 0.104 | 16.72 (0.01) | 2.11 (0.02) | 25.8 | 4.6 | 19.9 | 1.7 | | SE |
| 193 | | 10:30:04.3 | −35:32:52 | dE | 2 | 0.093 | 19.33 (0.04) | 1.37 (0.05) | 25.8 | 7.5 | 23.8 | 3.2 | | SE |
| 195 | | 10:30:06.4 | −35:18:25 | dE | 1 | 0.104 | 19.25 (0.04) | 1.62 (0.06) | 27.5 | 9.3 | 23.6 | 3.6 | | ELL, DM |
| 196 | | 10:30:06.4 | −35:23:31 | dE | 1 | 0.104 | 16.51 (0.01) | 1.83 (0.02) | 25.6 | 12.7 | 22.4 | 5.9 | | ELL, DM |
| 201 | | 10:30:13.6 | −35:15:54 | dE | 1 | 0.103 | 18.68 (0.03) | 1.74 (0.05) | 25.8 | 9.7 | 23.7 | 4.1 | | SE |
| 202 | | 10:30:15.3 | −35:27:32 | dE? | 3 | 0.099 | 19.64 (0.03) | 1.58 (0.04) | 25.8 | 5.5 | 23.7 | 2.6 | | SE |
| 203 | | 10:30:15.0 | −35:30:09 | d:E, N? | 3 | 0.095 | 16.36 (0.01) | 1.82 (0.02) | 25.8 | 10.8 | 21.1 | 3.6 | | SE,206 |
| 205 | | 10:30:18.4 | −35:24:43 | dE | 2 | 0.105 | 17.71 (0.01) | 2.02 (0.02) | 25.8 | 6.5 | 22.3 | 3.3 | | SE |
| 207 | | 10:30:18.4 | −35:31:26 | d:E, N | 2 | 0.094 | 15.71 (0.01) | 1.88 (0.02) | 25.8 | 10.6 | 20.8 | 4.1 | | SE |
| 208 | | 10:30:18.7 | −35:11:49 | S0(M32?) | 1 | 0.103 | 14.85 (0.01) | 1.95 (0.03) | 26.1 | 31.1 | 19.8 | 3.9 | 1774 ± 100[2] | ELL |
| | | | | | | | | | | | | | 1768 ± 83[3] | |
| 209 | | 10:30:19.4 | −35:34:48 | dE | 2 | 0.096 | 18.09 (0.02) | 1.72 (0.03) | 25.8 | 7.8 | 22.8 | 3.4 | | SE |
| 212 | | 10:30:21.3 | −35:35:31 | SmIII | 1 | 0.096 | 15.58 (0.01) | 1.31 (0.02) | 25.8 | 18.4 | 22.5 | 9.6 | | SE |
| 213 | | 10:30:21.6 | −35:12:14 | dE | 2 | 0.102 | 19.16 (0.03) | 1.66 (0.05) | 25.8 | 7.3 | 23.7 | 3.3 | | SE |
| 214 | | 10:30:22.5 | −35:30:32 | dE, N? | 2 | 0.095 | 18.71 (0.03) | 1.60 (0.04) | 25.8 | 8.2 | 23.5 | 3.7 | | SE, DM |
| 216 | | 10:30:22.5 | −35:10:26 | E | 2 | 0.102 | 16.15 (0.01) | 1.76 (0.02) | 25.8 | 7.8 | 20.3 | 2.7 | 2944 ± 103[3] | SE |
| 217 | | 10:30:23.2 | −35:37:08 | dE? | 3 | 0.097 | 19.98 (0.04) | 0.95 (0.05) | 25.8 | 5.5 | 24.4 | 3.0 | | SE |
| 220 | | 10:30:24.7 | −35:15:18 | S0/a | 1 | 0.102 | 14.16 (0.01) | 1.85 (0.02) | 28.3 | 30.3 | 20.7 | 8. 1 | 1223 ± 80[2] | ELL, DM |
| 221 | | 10:30:25.4 | −35:23:38 | dE | 2 | 0.109 | 19.22 (0.04) | 1.27 (0.05) | 25.8 | 8.2 | 24.1 | 3.8 | | SE |
| 222 | 3258B | 10:30:25.4 | −35:33:43 | S0/a | 2 | 0.095 | 14.15 (0.01) | 1.88 (0.02) | 25.8 | 20.9 | 20.9 | 8.9 | 2140 ± 80[2] | SE |
| 223 | | 10:30:25.6 | −35:13:19 | dE, N | 1 | 0.101 | – | – | – | – | – | – | – | BL |
| 224 | 3271 | 10:30:26.6 | −35:21:36 | SB02 | 1 | 0.108 | 11.13 (0.01) | 2.25 (0.02) | 27.3 | 116.5 | 19.4 | 18.4 | 3737 ± 27[2] | ELL, DM |
| | | | | | | | | | | | | | 3803 ± 31[3] | |
| 226 | 3273 | 10:30:29.2 | −35:36:36 | S0/a | 1 | 0.097 | 11.84 (0.01) | 2.23 (0.02) | 28.4 | 59.4 | 18.8 | 9.8 | 2419 ± 52[1] | ELL, DM |
| 227 | | 10:30:31.4 | −35:23:06 | dE? | 2 | 0.108 | 17.16 (0.01) | 1.78 (0.02) | 25.8 | 8.6 | 22.0 | 3.8 | | SE |
| 228 | | 10:30:31.6 | −35:14:38 | dE, N | 1 | 0.101 | 17.29 (0.02) | 1.78 (0.03) | 25.8 | 12.6 | 22.8 | 5.1 | | SE |
| 231 | | 10:30:34.5 | −35:23:13 | d:E, N | 1 | 0.108 | 14.98 (0.01) | 2.06 (0.02) | 25.8 | 11.3 | 20.4 | 4.8 | 2931 ± 80[2] | SE |
| | | | | | | | | | | | | | 2909 ± 38[3] | |
| 235 | | 10:30:39.6 | −35:31:44 | dE | 3 | 0.097 | – | – | – | – | – | – | – | DC |
| 237 | | 10:30:44.6 | −35:19:12 | dE, N? | 2 | 0.102 | 18.25 (0.02) | 1.69 (0.03) | 25.8 | 8.3 | 23.1 | 3.6 | | SE, DM |
| 238 | | 10:30:45.6 | −35:21:32 | Sm | 1 | 0.104 | 15.45 (0.01) | 1.47 (0.02) | 25.8 | 19.0 | 22.0 | 8.0 | | SE |
| 239 | | 10:30:47.5 | −35:28:55 | dE | 2 | 0.101 | 18.99 (0.03) | 1.52 (0.04) | 25.8 | 7.2 | 23.7 | 3.4 | | SE |
| 241 | | 10:30:48.4 | −35:32:20 | dE, N | 1 | 0.098 | 16.77 (0.02) | 1.84 (0.03) | 25.8 | 15.4 | 23.1 | 7.4 | | SE, DM |

*Notes*: Coordinates obtained through CDS, which are calculated from FS90. FS90 status 1 refers to definite members, status 2 to likely members and status 3 to possible members. $\mu_{T_1}$ corresponds to the threshold above which SEXTRACTOR detects and measures the object (MU_THRESHOLD), or to the surface brightness of the outermost isophote for ELLIPSE. $r_{T_1}$ is the radius that contains 90 per cent of the light for SEXTRACTOR. It is the equivalent radius ($r = \sqrt{ab} = a\sqrt{1-\epsilon}$) of the most external isophote for ELLIPSE. $\mu_{\rm eff}$ is obtained in both cases from $r_{\rm eff}$, the radius that contains one-half of the light. This radius is the output parameter HALF_LIGHT_RADIUS for SEXTRACTOR, and the equivalent effective radius for ELLIPSE. Radial velocities are from: 1 = NED, 2 = 6dF, 3 = our spectroscopic data. Remarks refers to: SE = magnitudes and colours measured with SEXTRACTOR; ELL = magnitudes and colours obtained from ELLIPSE; DM = doubtful morphology, i.e. FS90 morphology does not match our images morphology; DC = doubtful coordinates, i.e. FS90 coordinates do not clearly point to a galaxy; BL = bleeding; GAP = within a gap of the image; NS = nearby bright star; 206 = also designated FS90 206.

© 2008 The Authors. Journal compilation © 2008 RAS, MNRAS **386,** 2311–2322

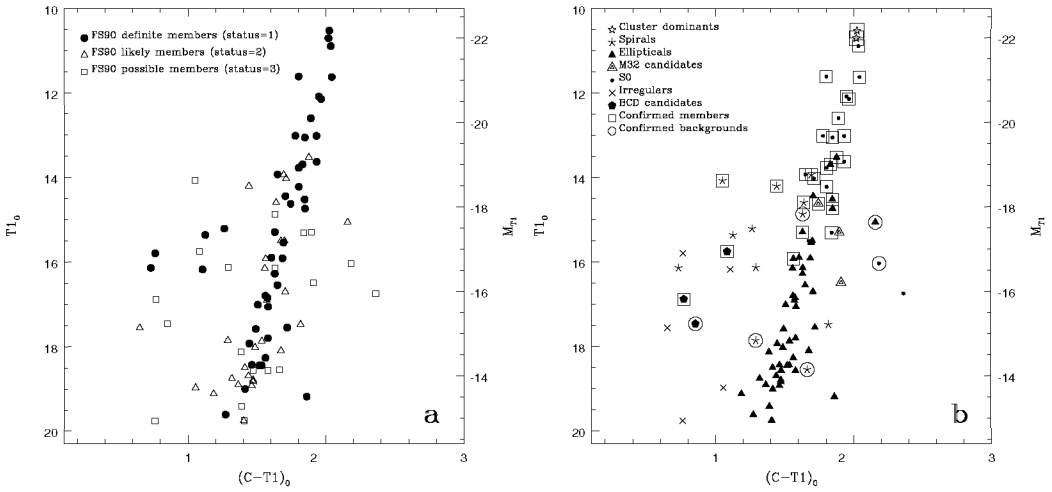


**Figure 2.** CMD of 93 FS90 galaxies in our central field of Antlia. $T_1$ magnitudes and $(C - T_1)$ colours are absorption and reddening corrected. (a) The membership status according to FS90 is shown. (b) Small symbols indicate different morphologies, and large open symbols identify spectroscopically confirmed Antlia members and background objects.

those obtained from NED,[1] and the last column shows some remarks.

Given that our sample covers a large luminosity range, it is interesting to estimate the signal-to-noise ratio (S/N) of one of the faintest and one of the brightest galaxies. For the *R* filter we have obtained an S/N within $r_{T_1}$ (as defined in the notes to Table 1) of about 100 for FS90 114, and S/N $\sim$ 16 000 for FS90 185 (NGC 3269). The S/N values of the *C* images are between one-half and one-third of the *R* images.

Taking as a reference the mean radial velocities of Antlia early- and late-type galaxies given by Hopp & Materne (1985) and considering a dispersion of $3\sigma$ from these values, we will consider as Antlia members all objects with velocities in the range 1200–4200 km s$^{-1}$. We prefer to take relaxed membership criteria given the substructure of the Antlia cluster and its probably complex dynamics. However, we note that, with the exception of four S0 galaxies with radial velocities below 2000 km s$^{-1}$, early-type galaxies with known radial velocities are confined in the range 2400–3900 km s$^{-1}$. We point out that 14 objects had radial velocities both from the literature and from our spectroscopic data. Our values are in quite good agreement with previous measurements as we obtain $\langle |V_{\rm lit} - V_{\rm ours}| \rangle = 63.5 \pm 55.9$ km s$^{-1}$.

Six galaxies out of the 100 FS90 objects present in our field have no photometric information: FS90 169 is located within a gap of the image, FS90 223 is affected by strong bleeding, FS90 148 is extremely faint and placed near a star, and three galaxies (viz. FS90 121, FS90 178 and FS90 235) have doubtful coordinates. Also FS90 203 and FS90 206 identify the same object.

## 3 COLOURS, MAGNITUDES AND SURFACE BRIGHTNESS

### 3.1 The colour–magnitude diagram

The left-hand panel of Fig. 2 plots our galaxies from Table 1 in the CMD according to their membership status given by FS90. Here the magnitudes and colours are reddening and absorption corrected according to the relation $A_R/A_V = 0.75$ (Rieke & Lebofsky 1985). We got the $A_V$ values by looking up the individual reddening values for the galaxies (Schlegel, Finkbeiner & Davis 1998) and using the relation $A_V = 3\,E(B - V)$. To transform $E(B - V)$ into $E(C - T1)$, we applied $E(C - T1) = 1.97\,E(B - V)$ (Harris & Canterna 1977).

In the right-hand panel of Fig. 2 we show the same galaxies, now indicating with different symbols their morphology. We distinguish spectroscopically confirmed Antlia members and background objects. We visually inspected all our FS90 objects in order to see if their morphologies match with those given by FS90. Although there is a general agreement, in a handful of cases they display doubtful morphologies (see the remarks in Table 1). In these cases they are displayed in the plots with their FS90 morphological classification. In this first analysis we are classifying galaxies simply as spirals (S), Es, S0s, BCDs and irregulars. A detailed morphological analysis will be given in a forthcoming paper.

In panel (a) we can see that almost all FS90 definite members define a quite narrow sequence. This sequence extends from the cluster dominant galaxies to the dwarf regime, with no visible change of slope and no increase in the scatter. Five deviant objects lie towards bluer colours. All are spirals or irregulars, supposedly star forming. Another object at the faint end (FS90 78, $T_1 \sim 19.2$, $(C - T_1) \sim 1.85$) shows a redder colour and is otherwise not remarkable. It is a nucleated dwarf galaxy extremely faint on the *C* image and its colour might not be trustworthy.

From panel (b), we see that practically all bright early-type galaxies with membership status 1 are spectroscopically confirmed members. The only elliptical which we spectroscopically confirmed as background galaxy, has membership 2 in FS90 and clearly deviates from the mean relation.

Three galaxies classified as BCD are found at intermediate brightness in the blue region. Two of them are spectroscopically confirmed Antlia members, while the faintest one is a background object. All three were considered to be status 3 members by FS90, given their morphologies. Our spectra, dominated by strong emission lines, at least confirm that they are indeed star forming.

In our field, FS90 also identified four objects as belonging to the very rare class of M32-type Es (e.g. Graham 2002; Mieske et al. 2005). One of them, rather classified as S0(M32?) (FS90 165), seems to be an S0 galaxy and it is shown with this morphology in Fig. 2.

[1] This research has made use of the NASA/IPAC Extragalactic Database (NED) which is operated by the Jet Propulsion Laboratory, California Institute of Technology, under contract with the National Aeronautics and Space Administration.

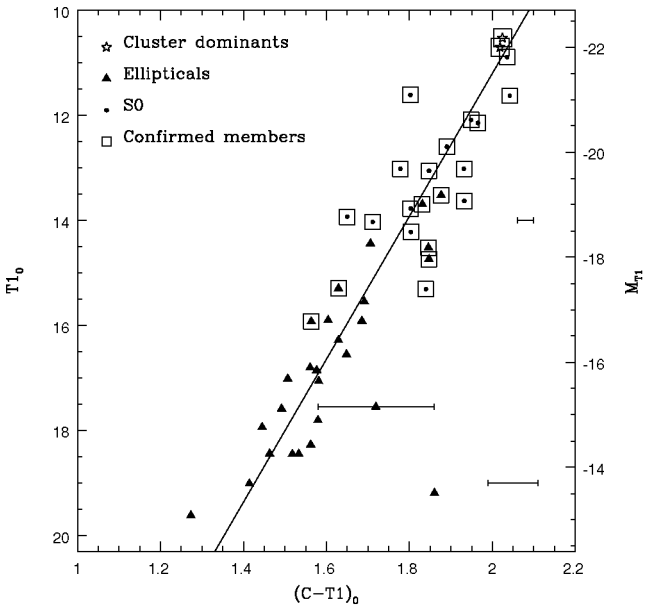


**Figure 3.** This plot shows only confirmed members and dwarf galaxies with a membership status of 1. The colour magnitude relation is tight for the fainter and broadens for brighter galaxies. The isolated error bars show typical colour errors corresponding to the range $10 < T_1 < 18$ (small) and $18 < T_1 < 20$ (large). We also display the error bar for the galaxy with the largest uncertainty.

Another one (FS90 208) is a confirmed member, but does not deviate strikingly from the mean CMR. The other two are too red for their brightness, or too faint for their colour, lying where background giant Es should be found. Although we have no radial velocities for them, their projected proximity to dominant Antlia galaxies, as well as their high surface brightness, lead us to consider them as M32-like candidates.

In Fig. 3 we show the positions of FS90 early-type galaxies (both E and S0) that are considered definite members of Antlia (i.e. FS90 status 1 early-type objects or galaxies that are spectroscopically confirmed members). Some galaxies are classified as SB0, and will be also included among the early-type galaxies.

We see a CMR that spans 9 mag without a perceptible change of slope. The faintest galaxies show a tight CMR, while the individual deviations among the brightest galaxies can be substantial. At the bright end, the S0 galaxies are slightly bluer on the average than the Es [$\langle (C-T_1)_0 \rangle_{S0} = 1.91 \pm 0.09$, $\langle (C-T_1)_0 \rangle_E = 1.94 \pm 0.10$] and display a larger dispersion about the mean relation. Without spectroscopic information one cannot interpret this difference in terms of age and/or metallicity (our medium-resolution spectra are suitable only to obtain radial velocities). However, since S0s are believed to be stripped spiral galaxies (e.g. Dressler et al. 1997), an age difference is most likely. Kuntschner (2000) has shown that, in the Fornax cluster, old stellar systems show tight scaling relations, and galaxies with young stellar populations tend to deviate from these relations. In particular, he found that S0s display luminosity-weighted ages less than those of Es, and show a considerable spread about the scaling relations.

We performed several least-squares fits to this relation, selecting the subsamples listed in Table 2. In all cases the fits were performed considering the uncertainties in both coordinates (Press et al. 1992), and rejecting the deviant faint object. From the fits we confirm that,

**Table 2.** Results of least-squares fits $T_{1_0} = a + b(C-T_1)_0$ performed to the absorption and extinction corrected CMR of early-type definite members of Antlia (i.e. early-type status 1 objects and early-type galaxies with radial velocities). The first column indicates the different samples and the second column gives the number of data points. The limit magnitude to separate bright and dwarf galaxies ($T_1 = 14$ mag) corresponds to $M_V \sim -18$ mag (Grebel 2005).

| Sample | Data | $a$ | $b$ | $\sigma_{(C-T_1)_0}$ |
|---|---|---|---|---|
| All definite members | 43 | $38.4 \pm 1.8$ | $-13.6 \pm 1.0$ | 0.07 |
| Bright definite members | 15 | $44.6 \pm 10.9$ | $-16.8 \pm 5.0$ | 0.07 |
| Dwarf definite members | 28 | $40.6 \pm 4.7$ | $-15.0 \pm 2.7$ | 0.08 |
| E definite members | 28 | $37.8 \pm 1.8$ | $-13.3 \pm 1.0$ | 0.07 |
| S0 definite members | 15 | $41.8 \pm 10.7$ | $-15.4 \pm 4.9$ | 0.09 |

within the uncertainties, all brightest galaxies follow the same relation as the rest of the early-type galaxies.

### 3.2 The surface brightness–luminosity diagram

Besides colours, relations between structural parameters of galaxies can also tell us about their evolutive status, serving, at the same time, to set membership criteria. For luminous ($M_B \lesssim -20$ mag) E galaxies, the effective radius $r_{\rm eff}$ tends to get larger while the mean effective surface brightness $\langle \mu_{\rm eff} \rangle$ (i.e. the mean surface brightness within $r_{\rm eff}$) gets fainter with increasing luminosity (e.g. Kormendy 1977).

Early-type dwarfs, however, are known to display a different trend (e.g. Ferguson & Binggeli 1994). This apparent dichotomy between low- and high-luminosity Es has been recently addressed by Graham & Guzmán (2003), who show that the general trend set by the fainter objects is broken by the very brightest Es.

Panel (a) of Fig. 4 plots $T_1$ versus $\langle \mu_{\rm eff} \rangle$ for all Antlia FS90 galaxies with their membership status indicated. As a reference we show two lines of constant effective radii, corresponding to 1.4 and 16 arcsec, obtained from the definition of mean effective surface brightness:

$$\langle \mu_{\rm eff} \rangle = T_1 + 2.5 \log \left(2\pi r_{\rm eff}^2\right). \quad (1)$$

Status 1 galaxies in the range $13 \lesssim T_1 \lesssim 17.5$ mag ($-19.7 \lesssim M_{T_1} \lesssim -15$) nicely follow the relation for a constant effective radius of $5.5 \pm 1.7$ arcsec. At the assumed Antlia distance 1 arcsec subtends 170 pc (Dirsch et al. 2003), giving a mean effective radius of $0.94 \pm 0.3$ kpc. Although our sample is small in the bright regime, there is a trend for the brightest galaxies to depart from the general relation, consistently with Graham & Guzmán (2003).

Status 2 galaxies are found more or less in the same regime, but status 3 galaxies are offset to brighter $\mu_{\rm eff}$, i.e. to smaller effective radii. This is consistent with the status assignment by FS90, i.e. more compact objects are given a lower probability of being members. Recently, Cellone & Buzzoni (2005) have confirmed a large background contamination among status 3 objects from FS90 in the NGC 5044 Group, which is at a similar distance as Antlia. A large fraction of background objects should thus be expected among status 3 galaxies in Fig. 4.

In panel (b) of Fig. 4, the morphological characteristics are indicated. The confirmed background objects are consistently found at lower $r_{\rm eff}$, as expected. Early- and late-type galaxies are not clearly separated, although the latter tend to show more diffuse structures. Note also the location of the three galaxies classified by FS90 as M32-like dwarf Es. While FS90 208 follows the same trend as the

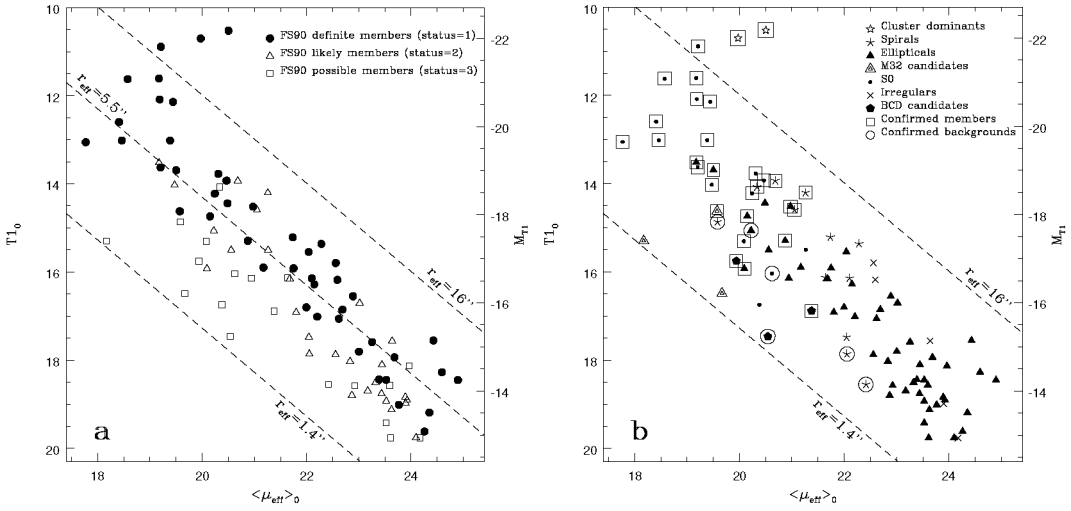


**Figure 4.** $T_1$ magnitude versus mean effective surface brightness. (a) The galaxies according to their membership status. Shown are three lines of different effective radius, the middle line indicating the mean value for galaxies fainter than $T_1 = 13$ mag. On the average, less likely members are displaced towards smaller effective radii. Status 2 members scatter around a constant effective radius. (b) The different morphologies are indicated. Two M32-like candidates and one background blue compact galaxy set the lowest limit in effective radii of our sample.

normal early-type galaxies, our M32-like candidates depart towards fainter magnitudes or higher surface brightness.

## 4 DISCUSSION

### 4.1 Surface brightness and effective radius

Fig. 4 shows that the mean relation between $T_1$ and $\langle\mu_{\rm eff}\rangle$ is to a good approximation the locus of a constant mean $r_{\rm eff}$. In other words, the mean $r_{\rm eff}$ is largely independent from luminosity. As a comparison, the Virgo dwarf galaxy sample by Binggeli & Cameron (1991), for example, exhibits the scaling law (see also Ferguson & Binggeli 1994) $\langle\mu_{\rm eff}\rangle = 0.75M_B + 35.3$, meaning that $r_{\rm eff}$ grows with luminosity. To test if both relations are compatible, we applied a two-dimensional Kolmogorov–Smirnov test to the following data sets: the $\langle\mu_{\rm eff}\rangle$ of the Antlia dwarfs ($T1 > 14$) transformed into the B band by means of the relations depicted in Section 4.3, and the $\langle\mu_{\rm eff}\rangle$ obtained for the same galaxies but using the scaling law from Ferguson & Binggeli (transforming the $M_{\rm T1}$ magnitudes into $M_B$). We calculated the statistic $D$ (Press et al. 1992) and got a probability $p = 27$ per cent, which means that the hypothesis that these surface brightness versus magnitude relations are different is not significant. Qualitatively similar trends can be seen in many other studies of early-type dwarfs (e.g. Caldwell & Bothun 1987; Vader & Chaboyer 1994; Cellone 1999; Gutiérrez et al. 2004).

Our Antlia dEs, then, show a similar trend to the NGC 5044 Group sample of Cellone & Buzzoni (2005), where dwarf Es with disc-like structure tend to produce a slightly lower than unity slope. It will be interesting to test whether examples of these candidates to harassed disc galaxies do exist in the (presumably) dynamically younger Antlia cluster. A larger sample, as well as a careful evaluation of background contamination, incompleteness, and selection biases affecting the $\langle\mu_{\rm eff}\rangle$ versus luminosity relation will be necessary to further study this issue.

In any case, our data are in principle consistent with a nearly constant effective radius for dwarfs, and it is therefore interesting to compare our mean $r_{\rm eff}$ value with CCD photometry of recent samples in galaxy clusters. In Fig. 5 we plot data for dwarf galaxies in Virgo

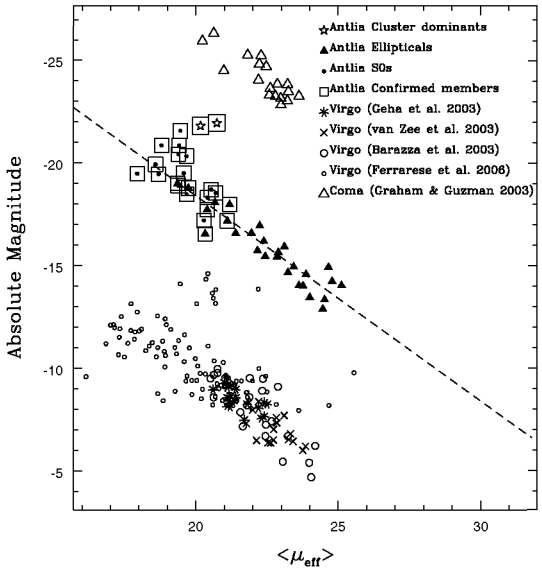


**Figure 5.** Absolute magnitude versus mean effective surface brightness for definite members of Antlia, and samples of Virgo and Coma galaxies. *The absolute mag scale is only valid for the Antlia galaxies*. The other samples are measured in other bands and most of them are shifted in mag to make the slopes better visible (the Virgo sample of Geha et al. (2003) by adding 8 mag, those of Barazza et al. (2003) and van Zee et al. (2004) by adding 9 mag, that from Ferrarese et al. (2006) by adding 7 mag, and the Coma sample (Graham & Guzmán 2003) by subtracting 7 mag). The dashed line is the locus of a constant effective radius of the Antlia galaxies. The slope for Coma, and that of Virgo for galaxies fainter than $\sim -13$ mag, are in agreement with a mean constant effective radius. The brightest galaxies from Ferrarese et al. (2006) follow the perpendicular behaviour of the brightest Antlia members, typical of core galaxies (Graham & Guzmán 2003).

(Barazza, Binggeli & Jerjen 2003; Geha, Guhathakurta & van der Marel 2003; van Zee et al. 2004) and in Coma (Graham & Guzmán 2003), where $\mu_{\rm eff}$ and $r_{\rm eff}$ are obtained model-independently, and we also add the ACS Virgo sample from Ferrarese et al. (2006). Since we are interested only in the slope of the relation between brightness

**Table 3.** Mean effective radius for the samples shown in Fig. 5. The fit to the ACS sample (Ferrarese et al. 2006) was performed rejecting the deviant point at −9.78 in absolute magnitude.

| Sample | Data | $D$ (Mpc) | $\langle r_{\rm eff}\rangle$ (kpc) |
|---|---|---|---|
| Antlia definite members ($T_1 > 13$ mag) | 36 | 35.2 | $0.94 \pm 0.3$ |
| Coma (Graham & Guzmán 2003) | 18 | 100 | $0.97 \pm 0.3$ |
| Virgo (Barazza et al. 2003) | 25 | 17 | $1.41 \pm 0.6$ |
| Virgo (Geha et al. 2003) | 17 | 17 | $0.96 \pm 0.2$ |
| Virgo (van Zee et al. 2004) | 16 | 17 | $1.14 \pm 0.3$ |
| Virgo (Ferrarese et al. 2006, $M_{\rm B} \gtrsim -20$) | 87 | 17 | $1.26 \pm 0.8$ |

and effective surface brightness, we just write *absolute magnitude* for the ordinate. The straight dashed line corresponds to the mean effective radius of Antlia early-type definite members with $T_1 > 13$ mag. The individual samples use different bands and we did not try to homogenize them.

Fig. 5 shows that all samples are consistent with our slope, pointing to a constant mean $r_{\rm eff}$. The ACS sample also agrees if we consider galaxies with absolute magnitudes fainter than −13 mag in our plot, except one deviant point at −9.78 in absolute magnitude. Note, however, that brighter Virgo galaxies follow the perpendicular relation defined by the Antlia brightest members, already reported by Graham & Guzmán (2003) for core galaxies. Considering distances of 17, 35.2 and 100 Mpc for Virgo, Antlia and Coma, respectively, we find the values listed in Table 3. These values are in quite good agreement, although with substantial dispersions.

It is thus tempting to test the potential of a constant $r_{\rm eff}$ as a distance indicator, in the light of previous efforts in the same direction (e.g. Binggeli & Jerjen 1998; Cellone 1999, and references therein). However, other samples with a similar luminosity coverage are desired to arrive at sensible conclusions.

### 4.2 M32-like objects

M32-like elliptical galaxies, which are distinguished by their low luminosity, compactness and high surface brightness, form a very rare class. Although there are many candidates catalogued up to now (see e.g. Binggeli et al. 1985), beside M32 (e.g. Graham 2002), only five other objects are confirmed as such (Chilingarian et al. 2007, and references therein). FS90 classified 13 galaxies as being M32-like in Antlia, four of which are placed in our field. As it was mentioned in Section 3.1, FS90 165 seems to be an S0 galaxy. A radial velocity is available only for the object FS90 208, which according to its surface brightness and effective radius seems to be a normal low luminosity E galaxy. The other two are FS90 110 and FS90 192.

It is noteworthy that, although their membership status has still to be settled, FS90 110 and FS90 192 lie close in projected distance to the two dominant galaxies, and display high surface brightness. These facts are consistent with what is found for all confirmed M32-like elliptical galaxies, except the doubtful case of object 1 from Mieske et al. (2005), which is about 5000 km s$^{-1}$ from the closest projected cluster giant elliptical. A detailed photometric analysis of Antlia M32 candidates will be given in a forthcoming paper.

### 4.3 Colour–magnitude relation

In order to compare our results with those reported in other papers, we obtained transformation equations from Johnson–Cousins magnitudes and colours into the Washington photometric system. To do so, we used the results of the population synthesis models of Buzzoni (2005), who gives broad-band colours in several photometric systems for template galaxies of different ages spanning the whole Hubble sequence. Linear relations with very low dispersions were obtained for homologous colour indices [e.g. $(B-R)$] versus $(C-T_1)$ while for colours probing different spectral regions [e.g. $(C-T_1)$ versus $(V-I_{\rm c})$] linear fits had to be restricted to the corresponding sets of galaxy types. These relations are

$$V = T_1 + (0.183 \pm 0.003)(C-T_1) + (0.208 \pm 0.003), \quad (2)$$

$$(C-T_1) = (2.548 \pm 0.040)(V-I_{\rm c}) - (1.482 \pm 0.038), \quad (3)$$

$$(B-R) = (0.701 \pm 0.006)(C-T_1) + (0.367 \pm 0.006). \quad (4)$$

By applying the SBF method and morphological classification to establish the membership status of Fornax dwarf galaxies, Hilker et al. (2003) and Mieske et al. (2007) have found a CMR for dEs with a scatter $\sigma_{(V-I)} = 0.14$ [$\sigma_{(C-T1)} \sim 0.36$] down to $V = 19$ mag ($T_1 \sim 18.6$ mag). In the Perseus cluster, early-type galaxies brighter than $M_B = -16$ mag ($T_1 \approx 15.3$ mag) display a tighter CMR with a scatter of $\sigma_{(B-R)} = 0.07$ [$\sigma_{(C-T_1)} \sim 0.1$], which is similar to our dispersion (Conselice et al. 2002). However, at $M_B = -13$ mag ($T_1 \approx 18.5$ mag), this scatter increases up to $\sigma_{(B-R)} = 0.54$ [$\sigma_{(C-T_1)} \sim 0.77$], i.e. there is no longer a relation.

López-Cruz et al. (2004, hereafter LC04) have studied the CMR for early-type galaxies in 57 X-ray detected Abell clusters in the redshift range $0.02 \leqslant z \leqslant 0.18$. They have found that the CMR is universal, with an average dispersion of $\sigma_{(B-R)} = 0.074 \pm 0.026$ [$\sigma_{(C-T_1)} \sim 0.1$]. When these authors distinguish between low- and high-redshift clusters, the mean dispersion turns to be 0.061 for clusters with $z < 0.04$, and 0.076 for the rest of the systems. Furthermore, LC04 noted that the cluster showing the largest dispersion in its CMR (A2152, $\sigma_{(B-R)} = 0.5$ at $R = 18$ mag) belongs to the set of systems that present background contamination from higher redshift clusters (see fig. 1 in their paper).

Regarding the slope of the relation in a $T_1$ versus $(C-T_1)$ diagram, LC04 find a range between −23.3 and −8.8 with a trend of steepening at increasing redshifts. In particular, the Coma cluster CMR spans 8 mag in $R$, down to $R = 21.2$, with a constant slope of −15.2. LC04 do not detect any significant change of slope within the CMR in any of their clusters.

For Fornax, Mieske et al. (2007) derived a slope which is equivalent to −12.1 in our CMD and, in the Perseus cluster, bright Es follow a relation with a slope of −12.6 (Conselice et al. 2002). Furthermore, Secker et al. (1997) find a CMR for the Coma cluster galaxies in the range $14 < R < 18.5$ mag, with a slope of −12.5 in a $T_1$ versus $(C-T_1)$ diagram. Data from a previous Washington system study of Fornax dwarf elliptical galaxies by Cellone, Forte & Geisler (1994), although spanning a small magnitude range, are still consistent with our Antlia slope.

Lisker et al. (2008) have recently obtained the CMR for dwarf early-type galaxies in the Virgo cluster, with SDSS data. In order to compare their slope with the one of our CMR, we transformed our mean relation to the SDSS photometry system using equation (2) quoted above, and equations (4) and (7) from Jordi, Grebel & Ammon (2006). We have obtained a value of $b = -0.022$ for a relation of the form $(g-r) = a + br$. This is in good agreement with what is obtained by Lisker et al. (2008) for their full dE sample [excluding dEs with blue centres, dE(bc)]. Our colour scatter transforms into $\sigma_{(g-r)} \sim 0.02$, which is smaller than those estimated by these authors.

From the previous analysis we can see that Antlia's CMR is one of the tightest and most extended relations reported up to now for nearby clusters, spanning a range of 9 mag from cD to dwarf galaxies. Our $\sigma_{(C-T_1)} \sim 0.07$ is consistent with the scatter reported by LC04 for 57 X-ray detected clusters, and with that found for Perseus in its bright end. The large scatter reported by Conselice et al. (2002, 2003) in the dwarf regime is probably due to background contamination as it was stated by LC04 (see also Penny & Conselice 2008). Antlia's CMR displays no change of slope in agreement with other clusters, and its slope is consistent with those found in Fornax, Virgo, Perseus and Coma.

It is interesting to note that our CMR slope is also in agreement with that reported, in the Washington photometric system, for the metal-poor (blue) GCs ($M_{T1} > -10.4$, $M_V > -10.0$) associated to NGC 4486 (Forte, Faifer & Geisler 2007). In this galaxy, the mean colour of the globulars becomes redder with increasing luminosity, a behaviour that has been called 'blue tilt' (Brodie & Strader 2006, and references therein). Forte et al. have found a slope of $-16.67$.

### 4.4 Luminosity–metallicity relation

To transform colours to metallicity, we naively adopt the relation given by Harris & Harris (2002) between $(C - T_1)$ and [Fe/H] derived for Galactic GCs. The transformation to our CMR then reads

$$[\mathrm{Fe/H}] = -2.71 + \sqrt{-4.10 - M_{T1}/1.88}. \quad (5)$$

However, this relation describes old, single population objects. A significant fraction of dE galaxies is known to harbour young or intermediate-age stellar populations (e.g. Cellone & Forte 1996), as well as hidden discs, bars, spiral structure (e.g. Drinkwater et al. 2001; Barazza, Binggeli & Jerjen 2002; De Rijcke et al. 2003; Graham, Jerjen & Luzmán 2003), or even ongoing star formation at their centres (e.g. Vigroux, Souviron & Vader 1984; Cellone & Buzzoni 2001; Lisker et al. 2006). van Zee et al. (2004) found in their sample of 16 Virgo dwarfs that all galaxies are dominated by populations in the age range 5–7 Gyr. The mean age of 17 dwarfs was found by Geha et al. (2003) to be 5 Gyr. Therefore, the integrated $(C - T_1)$ colours of dwarf galaxies are apparently determined by a mixture of age and metallicity, which we cannot disentangle.

Ignoring this complication, in Fig. 6 we plot the luminosity–metallicity relation of our Antlia galaxies. In order to compare our photometric metallicities with other samples, where mostly $M_V$ is given, we transformed our $T_1$ magnitudes to $M_V$, using equation (2). Equation (5) is shown as a reference with a solid line. We also plot Local Group dSphs from Grebel, Gallagher & Harbeck (2003), Virgo dwarf–globular transition objects (DGTOs) from Haşegan et al. (2005), Virgo dEs from Caldwell (2006), and the Fornax Compact Objects (FCO) from Mieske et al. (2006).

The individual scatter of the published metallicities around the mean relation is considerable and given the log–log character of this diagram, more than a global statement of the kind that low-mass galaxies are metal-poorer than high-mass galaxies is probably not permitted. It is more interesting to note how tight the relation for Antlia galaxies is in all its extension.

Three of the five brightest galaxies of the Local Group sample (viz. Sgr, NGC 185 and NGC 205) fall on the relation. The other two (M32 and NGC 147) depart towards higher luminosities or lower metallicities, as fainter dSphs do. However, given the large metallicity errors of the Local Group dSphs (a typical value is 0.4 dex, see Grebel et al. 2003), we cannot rule out that they follow the same trend as our mean luminosity–metallicity relation down to $M_V \sim -9$. Moreover, it should be noticed that this mean relation is just an extrapolation for magnitudes fainter than $M_V \sim -13$. In any case, irrespective of the curve defined by our mean relation in Fig. 6, dSphs seem to extend the luminosity–metallicity relation defined by the Antlia early-type galaxies, towards fainter magnitudes.

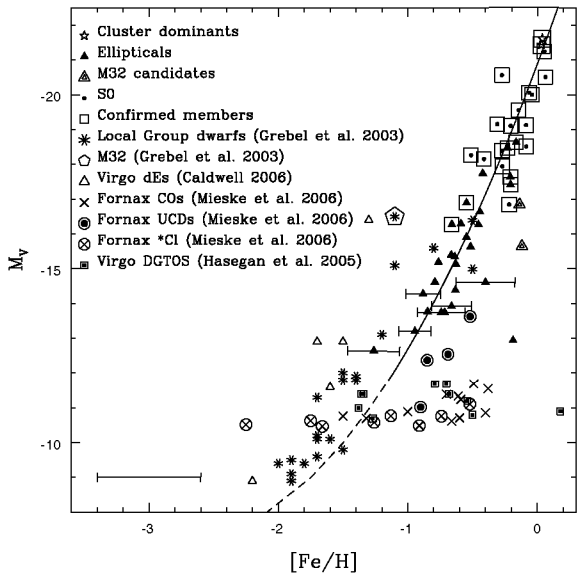


**Figure 6.** $M_V$ magnitude versus [Fe/H] for different samples. As a reference, we show our mean [Fe/H] versus $M_{T1}$ relation as a solid line, as well as its extrapolation as a dashed line. Our typical error in $(C - T_1)$ (0.02 mag) translates into a [Fe/H] error of 0.03 dex by means of equation (5). For clarity, we only show error bars for Antlia galaxies that display uncertainties greater than 0.1 dex. The large isolated error bar corresponds to the mean metallicity error in Grebel et al. (2003) sample (0.4 dex).

Virgo dEs seem to depart stronger from the Antlia mean relation than do the Local Group dSphs. Fornax and Virgo compact objects (COs and DGTOs), as well as Fornax bright GCs ($M_V < -10.4, \star$Cl) whose colour distribution is unimodal (e.g. Ostrov, Forte & Geisler 1998), do not obey any relation. Fornax Ultra Compact Dwarfs (UCDs) seem to follow the galaxies' trend, although towards fainter magnitudes or higher metallicities. This might be pointing to the galaxy nature of UCDs.

Given all the cautious remarks on the limited applicability of our photometric approach, Antlia galaxies define a tight luminosity–metallicity relation that extends over 9 mag and might be followed by Local Group dSphs in its faint end. We note that these faint objects would not show this trend if we had used a linear relation between Washington colour and metallicity.

The astrophysical meaning of such a relation, which covers giant Es, dwarfs and likely dwarf spheroidals has been discussed extensively in the literature. The formation history of these different types of galaxies is expected to be very different (e.g. De Rijcke et al. 2005). Dwarf Es probably were gas-rich late-type galaxies which lost their gas by stripping or outflows related to star formation activity (e.g. Mastropietro et al. 2005). Dwarf spheroidals may also have a tidal origin.

Finally, we remark that the bright S0s outnumber the elliptical galaxies roughly by a factor of 3. This is a difference to Fornax or Virgo, where most of the central galaxies are Es. If Es form by the merging of disc galaxies while S0s form by the gas removal of gas-rich disc galaxies, then merging was apparently much less efficient in Antlia than close encounters. Since S0s and Es most

certainly differ significantly in their population composition, a common metallicity–luminosity relation is not expected. S0s are thought to have a strong intermediate-age component, which is in line with the separation between S0s and Es in our diagrams. We have no handle on the metallicity without spectroscopic information, but we may suspect that age or composite populations are responsible for a large part of the scatter among the brightest galaxies.

## 5 CONCLUSIONS

We conclude that spectroscopically confirmed or FS90 definite (i.e. status 1) early-type dwarf members of the Antlia cluster define a very narrow sequence in the CMD. Luminous E and S0 galaxies follow the same CMR as their faint counterparts, with no perceptible change in slope and with a slightly larger dispersion, which is due to the separation of E and S0 galaxies.

This CMR spans 9 mag in brightness down to $T_1 = 19.7$ mag ($M_B \approx -11.7, M_V \approx -12.5$) with a small colour scatter of $\sigma_{(C-T_1)} \sim 0.07$ mag. Our relation for only dwarf galaxies is tighter [$\sigma_{(C-T_1)} \sim 0.08$mag] than that of most other samples found in the literature. This may be due to our homogeneous data, obtained thanks to the good match of our MOSAIC field to the angular size of the central region of Antlia. However, since there is the possibility that colours of dwarf galaxies may be influenced by younger stellar populations, one cannot be certain about metallicities, and part of the scatter might still be due to different mean ages.

The slope of the Antlia CMR is in agreement with those found in clusters like Fornax, Virgo, Perseus and Coma, despite of their different dynamical structure. This fact might indicate that the build-up of the CMR is more related to internal galaxy processes than to the influence of the environment. Furthermore, the slope of this relation is also consistent with that displayed by blue GCs ('blue tilt') in NGC 4486 (Forte et al. 2007). Previous comparisons between the 'blue tilt' and the positions of dE nuclei in the CMD, have already been performed by Harris et al. (2006) and Brodie & Strader (2006). As this subject is out of the scope of the present paper, we plan to go on studying it in the near future.

We find a clear relation between luminosity and effective surface brightness among the Antlia dwarf galaxies, scattering around a nearly constant mean effective radius with a mild (if at all) dependence on luminosity. A comparison with samples in the Virgo and Coma clusters reveals consistency with a mean effective radius of about 1 kpc for some samples. The dynamical meaning of this finding is unclear.

By applying the calibration between $(C - T_1)$ colours and [Fe/H] from Harris & Harris (2002), and interpreting the CMR as a metallicity–luminosity relation of old stellar systems, we find that Antlia early-type galaxies seem to follow a tight luminosity–metallicity relation that extends from cD galaxies to the dwarf regime. Within metallicity uncertainties, Local Group dSphs might extend this non-linear relation covering a range of 13 mag. Fornax UCDs seem to define a luminosity–metallicity relation as well, but towards fainter magnitudes or higher metallicities in comparison with that displayed by Antlia early-type galaxies and Local Group dSphs. This behaviour might point to a galaxy nature of UCDs.

The Antlia cluster provides a wealth of investigation possibilities which are still awaiting their exploitation. The present paper only refers to its central region and to early-type galaxies. In forthcoming papers, we shall give brightness profiles, present new dwarf galaxies and perform spectroscopic studies of Antlia galaxies. We also plan to study the M32 candidates as well as the UCD candidates that we might find in the Antlia fields.

## ACKNOWLEDGMENTS

The measurement of new radial velocities has been done by Cristian Aruta. We dedicate this paper to his memory.

We thank the referee for a thorough reading of the manuscript and for useful comments that helped to improve this paper. We also thank Nicola Masetti for kindly providing observing time. This work was funded with grants from Consejo Nacional de Investigaciones Científicas y Técnicas de la República Argentina, Agencia Nacional de Promoción Científica Tecnológica and Universidad Nacional de La Plata (Argentina). TR and LI are grateful for support from the Chilean Centre for Astrophysics, FONDAP No. 15010003. AVSC would like to thank Neil Nagar and Universidad de Concepción for their hospitality during her stay in Chile, where part of this work was done.

## REFERENCES

Adami C. et al., 2006, A&A, 459, 679
Andreon S., Cuillandre J.-C., Puddu E., Mellier Y., 2006, MNRAS, 372, 60
Barazza F. D., Binggeli B., Jerjen H., 2002, A&A, 391, 823
Barazza F. D., Binggeli B., Jerjen H., 2003, A&A, 407, 121
Bassino L. P., Richtler T., Dirsch B., 2008, MNRAS, in press (arXiv:0802.2354)
Baum W., 1959, PASP, 71, 106
Bertin E., Arnouts S., 1996, A&AS, 117, 393
Binggeli B., Cameron L. M., 1991, A&A, 252, 27
Binggeli B., Jerjen H., 1998, A&A, 333, 17
Binggeli B., Sandage A., Tammann G. A., 1985, AJ, 90, 1681
Bower R. G., Lucey J. R., Ellis R. S., 1992, MNRAS, 254, 601
Brodie J. P., Strader J., 2006, ARA&A, 44, 193
Buzzoni A., 2005, MNRAS, 361, 725
Caldwell N., 1983, AJ, 88, 804
Caldwell N., 2006, ApJ, 651, 822
Caldwell N., Bothun G. D., 1987, AJ, 94, 1126
Canterna R., 1976, AJ, 81, 228
Carrasco E. R., Mendes de Oliveira C., Infante L., 2006, AJ, 132, 1796
Carter D. et al., 2002, ApJ, 567, 772
Cellone S. A., 1999, A&A, 345, 403
Cellone S. A., Buzzoni A., 2001, A&A, 369, 742
Cellone S. A., Buzzoni A., 2005, MNRAS, 356, 41
Cellone S. A., Forte J. C., 1996, ApJ, 461, 176
Cellone S. A., Forte J. C., Geisler D., 1994, ApJS, 93, 397
Chang R., Gallazzi A., Kauffmann G., Charlot S., Ivezić Ž., Brinchmann J., Heckman T., 2006, MNRAS, 366, 717
Chilingarian I., Cayatte V., Chemin L., Durret F., Laganá T. F., Adami C., Slezak E., 2007, A&A, 466, L21
Conselice C. J., Gallagher J. S., Wyse R. F. G., 2002, AJ, 123, 2246
Conselice C. J., Gallagher J. S., Wyse R. F. G., 2003, AJ, 125, 66
De Rijcke S., Dejonghe H., Zeilinger W. W., Hau G. K. T., 2003, A&A, 400, 119
De Rijcke S., Michielsen D., Dejonghe H., Zeilinger W. W., Hau G. K. T., 2005, A&A, 438, 491
De Vaucouleurs G., 1961, ApJS, 5, 233
Dirsch B., Richtler T., Bassino L. P., 2003, A&A, 408, 929
Dressler A., 1984, ApJ, 286, 97
Dressler A. et al., 1997, ApJ, 490, 577
Drinkwater M. J., Gregg M. D., Holman B. A., Brown M. J. I., 2001, MNRAS, 326, 1076
Ferguson H. C., Binggeli B., 1994, A&AR, 6, 67
Ferguson H. C., Sandage A., 1990, AJ, 100, 1
Ferrarese L. et al., 2006, ApJS, 164, 334
Forte J. C., Faifer F. R., Geisler D., 2007, MNRAS, 382, 1947
Geha M., Guhathakurta P., van der Marel R. P., 2003, AJ, 126, 1794
Geisler D., 1996, AJ, 111, 480
Graham A. W., 2002, ApJ, 568, L13

Graham A. W., Driver S. P., 2005, PASA, 22, 118
Graham A. W., Guzmán R., 2003, AJ, 125, 2936
Graham A. W., Jerjen H., Guzmán R., 2003, AJ, 126, 1787
Grebel E. K., 2005, in Jerjen H., Binggeli B., eds, Proc. IAU Colloq. 198, Near-Field Cosmology with Dwarf Elliptical Galaxies. Cambridge Univ. Press, Cambridge, p. 1
Grebel E. K., Gallagher J. S., Harbeck D., 2003, AJ, 125, 1926
Gutiérrez C. M., Trujillo I., Aguerri J. A. L., Graham A. W., Caon N., 2004, ApJ, 602, 664
Harris H. C., Canterna R., 1977, AJ, 82, 798
Harris W. E., Harris G. L. H., 2002, AJ, 123, 3108
Harris W. E., Whitmore B. C., Karakla D., Okoń W., Baum W. A., Hanes D. A., Kavelaars J. J., 2006, ApJ, 636, 90
Haşegan M. et al., 2005, ApJ, 627, 203
Hilker M., Mieske S., Infante L., 2003, A&A, 397, L9
Hopp U., Materne J., 1985, A&AS, 61, 93
Jordi K., Grebel E. K., Ammon K., 2006, A&A, 460, 339
Kodama T., Arimoto N., 1997, A&A, 320, 41
Köppen J., Weidner C., Kroupa P., 2007, MNRAS, 375, 673
Kormendy J., 1977, ApJ, 217, 406
Kuntschner H., 2000, MNRAS, 315, 184
Lisker T., Grebel E. K., Binggeli B., 2005, in Jerjen H., Binggeli B., eds, Proc. IAU Colloq. 198, Near-Field Cosmology with Dwarf Elliptical Galaxies. Cambridge Univ. Press, Cambridge, p. 311
Lisker T., Glatt K., Westera P., Grebel E. K., 2006, AJ, 132, 2432
Lisker T., Grebel E. K., Binggeli B., 2008, AJ, 135, 380
López-Cruz O., Barkhouse W. A., Yee H. K. C., 2004, ApJ, 614, 679 (LC04)
Mastropietro C., Moore B., Mayer L., Debattista V. P., Piffaretti R., Stadel J., 2005, MNRAS, 364, 607
Mieske S., Infante L., Hilker M., Hertling G., Blakeslee J. P., Benítez N., Ford H., Zekser K., 2005, A&A, 430, L25
Mieske S., Hilker M., Infante L., Jordán A., 2006, AJ, 131, 2442
Mieske S., Hilker M., Infante L., Mendes de Oliveira C., 2007, A&A, 463, 503
Nakazawa K., Makishima K., Fukazawa Y., Tamura T., 2000, PASJ, 52, 623
Nonino M. et al., 1999, A&AS, 137, 51
Ostrov P., Forte J. C., Geisler D., 1998, AJ, 116, 2854
Pedersen K., Yoshii Y., Sommer-Larsen J., 1997, ApJ, 485, L17
Penny S. J., Conselice C., 2008, MNRAS, 383, 247
Press W. H., Teukolsky S. A., Vetterling W. T., Flannery B. P., 1992, in Numerical Recipes in FORTRAN: The Art of Scientific Computing, 2nd edn. Cambridge Univ. Press, Cambridge
Prugniel P., Simien F., 1996, A&A, 309, 749
Rakos K., Schombert J., Maitzen H. M., Prugovecki S., Odell A., 2001, AJ, 121, 1974
Rieke G. H., Lebofsky M. J., 1985, ApJ, 288, 618
Schlegel D., Finkbeiner D., Davis M., 1998, ApJ, 500, 525
Secker J., Harris W. E., Plummer J. D., 1997, PASP, 109, 1377
Terlevich A. I., Forbes D. A., 2002, MNRAS, 330, 547
Terlevich A. I., Caldwell N., Bower R. G., 2001, MNRAS, 326, 1547
Thomas D., Bender R., Hopp U., Maraston C., Greggio L., 2003a, Ap&SS, 284, 599
Thomas D., Maraston C., Bender R., 2003b, MNRAS, 343, 279
Tonry J. L., Dressler A., Blakeslee J. P., Ajhar E. A., Fletcher A. B., Luppino G. A., Metzger M. R., Moore C. B., 2001, ApJ, 546, 681
Vader J. P., Chaboyer B., 1994, AJ, 108, 1209
van Zee L., Barton E. J., Skillman E. D., 2004, AJ, 128, 2797
Vazdekis A., Kuntschner H., Davies R. L., Arimoto N., Nakamura O., Peletier R., 2001, ApJ, 551, L127
Vigroux L., Souviron J., Vader J. P., 1984, A&A, 139, L9
Visvanathan N., Sandage A., 1977, ApJ, 216, 214

This paper has been typeset from a TEX/LATEX file prepared by the author.